Report
R-21-15
December 2021

Local depletion of aqueous manganese and its correlation with manganese oxidizing bacteria and precipitates in the Äspö bedrock

Daniel Svensson
Linda Alakangas
Birgitta Kalinowski
Stephanie Turner
Mark Dopson
Magnus Ståhle

SVENSK KÄRNBRÄNSLEHANTERING AB

SWEDISH NUCLEAR FUEL
AND WASTE MANAGEMENT CO

Box 3091, SE-169 03 Solna
Phone +46 8 459 84 00
skb.se

SVENSK KÄRNBRÄNSLEHANTERING

ISSN 1402-3091
SKB R-21-15
ID 1953183
December 2021

Local depletion of aqueous manganese and its correlation with manganese oxidizing bacteria and precipitates in the Äspö bedrock

Daniel Svensson, Linda Alakangas, Birgitta Kalinowski
Svensk Kärnbränslehantering AB

Stephanie Turner, Mark Dopson, Magnus Ståhle
Linnaeus University

Keywords: Manganese, Bacteria, Groundwater.

This report is published on www.skb.se

© 2021 Svensk Kärnbränslehantering AB

Abstract

The deep biosphere contains active microorganisms from all three domains of life that drive global biogeochemical cycles including metals such as manganese (Mn) and iron (Fe) that can also act as electron donors and/or acceptors for microbial growth. Black precipitates were observed in waters emanating from the Äspö Hard Rock Laboratory tunnel wall at several sites that were hypothesized to be due to manganese precipitates formed as a result of microbial mediated Mn(II)-oxidation. This has never been investigated before, despite the fact that the black deposits have been observed for several years and occur in several places in the tunnel. The study was mainly conducted for general process understanding in the deep geosphere and could potentially be relevant in the safety assessment. Due to the importance of Mn for many organisms, the precipitates were investigated and the microbial communities characterized to determine if the environment contained Mn(II)-oxidizing taxa. The water emanating from the tunnel wall was determined to be of mixed origin potentially containing glacial meltwater that was depleted in manganese. Solid phase analysis showed high levels of Mn and calcium (Ca) and that the surface was covered with a 200 µm thick amorphous or poorly crystalline Mn-mineral on top of calcite and then crystalline rock. High throughput 16S rRNA gene sequencing of the microbial community identified disparate communities between the water, mineral, and sediment. The microbial community of all solid and liquid samples was dominated by the phylum Proteobacteria while 16S rRNA gene sequences most similar to characterized Mn(II)-oxidizers included *Hyphomicrobium* amplicon sequencing variants (ASVs) identified in waters, sediment, and precipitates. In addition, 16S rRNA sequences that aligned with the Mn(II)-oxidizing genera *Pseudonocardia* and *Mycobacterium* had a higher relative abundance in the precipitates. The data suggest that the precipitates from the Äspö Hard Rock Laboratory tunnel were enriched in Mn and that the microbial characterization identified 16S rRNA gene sequences that aligned with known Mn(II)-oxidizing taxa. Manganese oxides may, along with iron oxides, act as a sink for rare earth elements (REEs) that in turn could be of interest for the general understanding of the cycling of such elements in the deep subsurface.

Contents

1 Introduction

Waters containing black precipitates ('black water') have been observed to leach from tunnel walls in the Äspö Hard Rock Laboratory (HRL; Figure 1-1). In order to understand the various ongoing processes that could affect the groundwater chemistry it was decided to investigate the nature and origin of the black precipitates at Äspö HRL as this potentially could also occur in Forsmark. A similar phenomenon has been observed at the Ytterby mine (Sweden) where a manganese (Mn) oxide enriched in yttrium and rare earth elements (REE) precipitated as a result of microbial activity (Sjöberg 2019). In general, Mn(II)-oxidizing bacteria are phylogenetically diverse and have been identified from different lineages including Proteobacteria, Firmicutes, and Actinobacteria (Tebo et al. 2005). Microbes identified in the Ytterby mine biofilm that have been shown to oxidize Mn(II) include *Hydrogenophaga* sp., *Pedobacter* sp., *Rhizobium* sp., and *Nevskia* sp. along with the fungus *Cladosporium* sp. (Sjöberg 2019).

Figure 1-1. *The four Äspö HRL TAS04 sampling sites. A – left end corner (site LE), B – right end corner (site RE), C – left middle wall (site LM), and D – right middle wall (site RM).*

The objective of this study was to determine the process causing the black precipitates in the water leaching from the tunnel walls at the Äspö HRL. Based on the results of the study at the Ytterby mine (Sjöberg 2019), it was hypothesized that the black precipitates were the result of microbial Mn(II) oxidation as the environment was aerobic and the water did not have the typical smell of hydrogen sulfide from sulfate reduction. In this study, we report chemical analyses of the water plus the black precipitates, microscopy images of two 'black waters', and a 16S rRNA gene amplicon survey to investigate if samples contain microbial species known to oxidize Mn(II).

2 Methods

2.1 Sample collection

Samples were collected at four sites within the TAS04 tunnel at Äspö HRL at approximately 400 m depth (Table 2-1 and Figure 1-1). Flowing water was sampled at two sites (left end, LE and right end, RE) where the rock was blackish. Microbial cells were collected from triplicate water samples (i.e. triplicate biological replicates of 50 mL each) with a sterile syringe, filtered through a 0.1 µm filter (Durapore® membrane filter, Merck Millipore Ltd.) connected to the syringe, and the filter placed in a sterile cryo-tube. Sediment was sampled from the small pool at site RE with a sterile spoon. In addition, black precipitates were scraped from the wall with a sterile spatula at all four sites (sites LE and RE plus sites left middle, LM, and right middle, RM, wall). Water samples for DNA extraction were taken in November 2019, whereas sediment and the black precipitates were sampled in December 2020. All samples for DNA extraction were immediately frozen in liquid nitrogen, transported back to the laboratory, and stored at −20 °C until processing.

2.2 Water chemistry analyses

Water samples (site LE and site RE) for chemical analysis were collected in bottles and filtered (0.45 µm) according to standard SKB protocols listed in Table 3-1 and Table 3-2, and analyzed for pH, conductivity, carbonate alkalinity, anions, DOC/TOC (dissolved organic carbon/total organic carbon), O^{18}, and deuterium (D). Analysis for Mn was done by ALS Scandinavia using ICP-AES.

2.3 Solid phase analyses

2.3.1 Sampling of rock and scanning electron microscopy

Crystalline rock covered by a black surface mineralization (black precipitates) was sampled close to TAS04, at approximately 400 m depth in the Äspö HRL tunnel. The rock was cut into a slice using a standard rock saw. The approximate size of the slice was [2 × 2 × 0.5] cm^3.

The morphology and elemental composition of the rock sample was examined using SEM-EDS (Scanning Electron Microscopy – Energy Dispersive X-ray Spectrometry) on a Hitachi TM4000 Plus SEM with a Bruker SCU (Scanning Control Unit) EDS detector. The sample was air dried and mounted on conductive tape prior analysis. The sample was not embedded or coated. Standard settings from the manufacturer optimized for EDS were used (25 keV). The EDS evaluation was performed using the standards included in the software provided by the manufacturer. The EDS detector is calibrated on a routine basis at the laboratory.

2.3.2 X-ray fluorescence spectroscopy

X-ray fluorescence (XRF) spectroscopy was used to determine the chemical composition of the sample surface using a Panalytical Epsilon spectrometer equipped with an Rh X-ray tube. The measurement setup and evaluation were using the Panalytical Epsilon 3 software with the included Omnian standard. The agate mortar milled sample was placed on a mylar foil as a powder for the analysis. Note that the XRF setup used was not able to determine the content of elements with an atomic number lower than sodium. The elemental content is reported as e.g. oxides and the sum is normalized to 100 %.

2.3.3 Powder X-ray diffraction

Powder X-ray diffraction (XRD) was applied in order to characterize crystalline phases in the sample. The equipment used was a Panalytical XPert diffractometer equipped with a Co X-ray tube and a PIXcel detector. A programmable divergence slit was used and data collected in the interval of 4–100 degrees two theta. The samples were milled in an agate mortar prior to the analysis. A zero background silicon substrate was used as a sample holder.

2.4 Microbiology

Microbial communities can be investigated by next generation DNA sequencing of 16S rRNA gene amplicons (a piece of the 16S rRNA gene that has been amplified by polymerase chain reaction, PCR) that provides information on the microbial community structure of a given sample. Advantages of this method include that it rapidly provides tens of thousands of sequences per sample that gives an accurate snapshot of the community at the time of sampling. However, the method suffers from PCR amplification bias that can alter the given community structure as well as fail to amplify certain taxa. For instance, although the PCR primers used in this study amplify some archaeal taxa, they are known to have a bias towards bacterial species (Hugerth et al. 2014).

2.4.1 Microbial microscopy

Separate samples were collected for microscopy in October 2019. Therefore, flowing water as well as a portion of the black precipitates from the rock were sampled at sites LE and RE (Table 2-1). Samples for cell counts were fixed with 1 % (vol/vol) formaldehyde solution and stored at 4 °C. The fixed sample was filtered on a NucleporeTM black polycarbonate membrane filter (0.22 µm; GE Healthcare WhatmanTM), stained with SYBR Green I (InvitrogenTM), and analyzed by epifluorescence microscopy (Olympus BX50).

Table 2-1. Sample overview for the microbiological analyses.

Sample name	Site	Sample type	Replicate
TAS04_LE_W1	TAS04 left end corner (LE)	Water (W)	#1
TAS04_LE_W2	TAS04 left end corner (LE)	Water (W)	#2
TAS04_LE_W3	TAS04 left end corner (LE)	Water (W)	#3
TAS04_RE_W1	TAS04 right end corner (RE)	Water (W)	#1
TAS04_RE_W2	TAS04 right end corner (RE)	Water (W)	#2
TAS04_RE_W3	TAS04 right end corner (RE)	Water (W)	#3
TAS04_RE_S1	TAS04 right end corner (RE)	Sediment (S)	#1
TAS04_RE_S2	TAS04 right end corner (RE)	Sediment (S)	#2
TAS04_RE_BP	TAS04 right end corner (RE)	Black precipitates (BP)	#1
TAS04_LM_BP	TAS04 left middle wall (LM)	Black precipitates (BP)	#1
TAS04_RM_BP	TAS04 right middle wall (RM)	Black precipitates (BP)	#1

2.4.2 DNA extraction

Genomic DNA from cells captured on the 0.1 µm filters was extracted using the DNeasy PowerWater Kit (Qiagen). Genomic DNA from sediment samples and black precipitates was extracted using the DNeasy PowerSoil Kit (Qiagen). DNA extraction was performed according to the manufacturer´s instructions except that the final DNA was eluted in 50 µL of elution buffer.

2.4.3 16S rRNA amplicon sequencing and bioinformatics

Partial 16S rRNA genes were amplified with a modified PCR protocol from Hugerth et al. (2014) using primers 341F and 805R (Herlemann et al. 2011). It should be noted that the PCR primers used in this study were designed to amplify bacteria although some archaeal lineages are amplified from Äspö HRL groundwaters (Lopez-Fernandez et al. 2018a, b). However, as noted above, not all archaeal lineages will be amplified or with an equal efficiency as for the bacteria. PCR amplification and Illumina libraries were constructed and sequenced at Science for Life Laboratory, Sweden (www.scilifelab.se) according to Lindh et al. (2015). The DADA2 pipeline (version 1.16; Callahan et al. 2016) was used to process the sequence data. The obtained amplicon sequencing variants (ASVs; single unique 16S rRNA gene DNA sequences recovered from the analysis of the Illumina

sequencing) were annotated against the Genome Taxonomy Database (GTDB release 202; Parks et al. 2018), and finally analyzed and visualized in R (version 3.6.3; R Core Team 2019). Plots were created with the R package 'ggplot2' (version 3.3.2, Wickham 2016). Alpha (within-sample) and beta (between-sample) diversity were analyzed with the 'vegan' package (version 2.5–6; Oksanen et al. 2020). For analysis of beta diversity, a non-metric multidimensional scaling (NMDS) was applied with default settings based on a Bray Curtis dissimilarity matrix using relative abundances of the ASVs. To test for significant differences between sample types, a PERMANOVA was used ('adonis' function from R package 'vegan'). Prior to PERMANOVA, the homogeneity of within-group dispersion was checked (function 'betadisper') and was found to be not significantly different between sample types.

3 Results and discussion

3.1 Water chemistry analyses

The chemical parameters that were analyzed are presented in Tables 3-1 and 3-2.

Table 3-1. Chemistry data from the wall.

Analysis	Result	Unit	Uncertainty	Day of analysis
pH (25 °C)	7.45	pH	± 0.10	2019-12-02
Conductivity	1 180	mS/m	± 59.0	2019-12-02
Carbonate alkalinity	32.0	mg/L	± 1.645	2019-12-02
Manganese	0.061	mg/L	± 0.004	2019-12-02
Fluoride potentiometric	1.6	mg/L	± 0.384	2019-12-02
Chloride potentiometric	3 830	mg/L	± 229.8	2019-12-02
Bromide_IC	18.3	mg/L	± 2.745	2019-12-02
Sulfate_IC	276	mg/L	± 33.12	2019-12-02
Smell	Non specific	-	-	2019-12-02
$\delta^{2}H$	−85.7	‰(VSMOW)	± 1.5	2019-12-02
$\delta^{18}O$	−11.67	‰(VSMOW)	± 0.2	2019-12-02
DOC	2.5	mg/L	± 0.25	2019-12-02
TOC	2.5	mg/L	± 0.25	2019-12-02

Table 3-2. Chemistry data from the pond.

Analysis	Result	Unit	Uncertainty	Day of analysis
pH (25 °C)	7.56	pH	± 0.10	2019-12-02
Conductivity	1 310	Ms/m	± 65	2019-12-02
Carbonate alkalinity	42.6	mg/L	± 2.13	2019-12-02
Manganese	0.082	mg/L	± 0.006	2019-12-02
Fluoride potentiometric	1.5	mg/L	± 0.36	2019-12-02
Chloride potentiometric	3 830	mg/L	± 229.8	2019-12-02
Bromide_IC	18.8	mg/L	± 2.82	2019-12-02
Sulfate_IC	278	mg/L	± 33.36	2019-12-02
Smell	Non specific	-	-	2019-12-02
$\delta^{2}H$	−85.8	‰(VSMOW)	± 1.5	2019-12-02
$\delta^{18}O$	−11.84	‰(VSMOW)	± 0.2	2019-12-02
DOC	2.4	mg/L	± 0.25	2019-12-02
TOC	2.7	mg/L	± 0.25	2019-12-02

The ‘black water’ is defined as a mixed water type (Figure 3-1), meaning that the water is an unknown mixture of waters from different origin based on the ^{18}O and ^{2}H isotopes. The chloride concentration of 3 800 mg/ L indicates contribution of a water of marine origin and the isotope signature suggests some contribution from glacial origin or/and saline interference (Mathurin et al. 2012) and differ from other boreholes sampled around or nearby TAS04 in the monitoring program (Figure 3-1).

The chemistry analysis indicated that the water was depleted in Mn and has oxidized compared to waters from boreholes at different depths and origin (Figure 3-1). The monitoring data can be found in the SKB database SICADA.

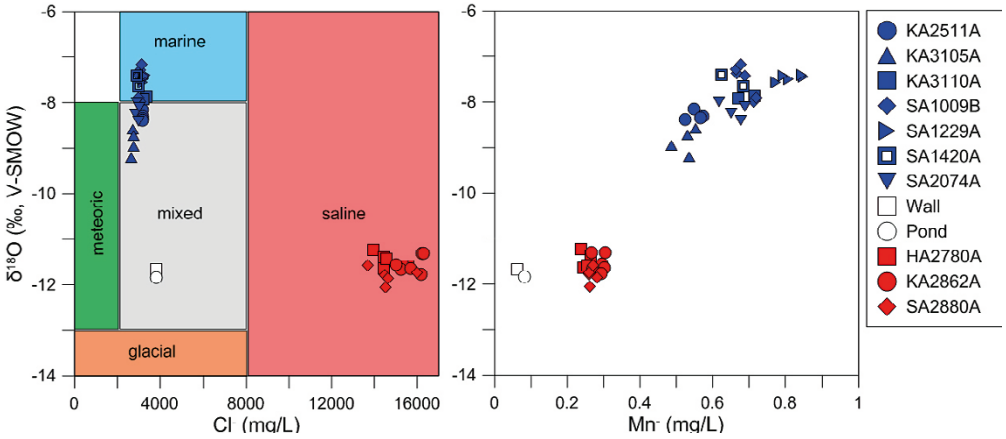

Figure 3-1. *The black water from the wall and pond in TAS04 (white symbols) is a mixed water, possibly with some contribution from glacial origin or/and saline interference (Mathurin et al. 2012). Saline surrounding waters in Äspö HRL are indicated with red symbols and have high chloride and low ^{18}O, and the blue symbols are water with high marine signature due to low Cl and high ^{18}O. Even though the black water in TAS04 has low Cl indicated a marine mixed water the Mn is low and also lower compared to a saline water with low ^{18}O.*

3.2 Solid phase analyses

3.2.1 Scanning electron microscopy

The surface had few morphological features at low magnification in the SEM (Figure 3-2). A number of spot analyses (n = 4) were performed on the surface showing high levels of Mn and Ca while the levels of Fe, Si, Al, and Na were low (Table 3-3).

Figure 3-2. *Surface of black mineralization visualized by SEM.*

From the side the surface was somewhat brighter compared to the inner rock in back scattered electrons mode (Figure 3-3). This indicated that the average atomic number of the surface was higher compared to the crystalline rock, with the exception of some very bright sporadically distributed spots. An EDS map covering a somewhat smaller area showed that the surface mineralization was dominated by a 200 µm thick layer of Mn-mineral (potentially an oxide and/or hydroxide), followed by a 200 µm layer of a Ca-mineral (potentially calcite), and then the crystalline rock (Table 3-3 and Figure 3-4). The crystalline rock was in some areas high in Si (potentially quartz), Al and Na (potentially albite), and Fe (potentially hematite and/or magnetite).

Table 3-3. Elemental spot analysis on different sites on the surface using SEM/EDS.

Site	Na	Al	Si	Cl	Ca	Mn	Fe
80	0.40	0.44	1.48	b.d	8.56	6.85	0.71
81	b.d	b.d	1.14	0.10	10.68	6.50	b.d.
82	b.d.	b.d.	0.93	b.d.	11.81	5.98	b.d.
83	b.d.	b.d.	1.07	b.d.	10.55	7.16	0.49
Mean	0.40	0.44	1.16	0.10	10.40	6.62	0.60
Sigma	0.000	0.000	0.234	0.000	1.352	0.507	0.156
SigmaMean	0.000	0.000	0.117	0.000	0.676	0.254	0.078

b.d. = below detection limit.

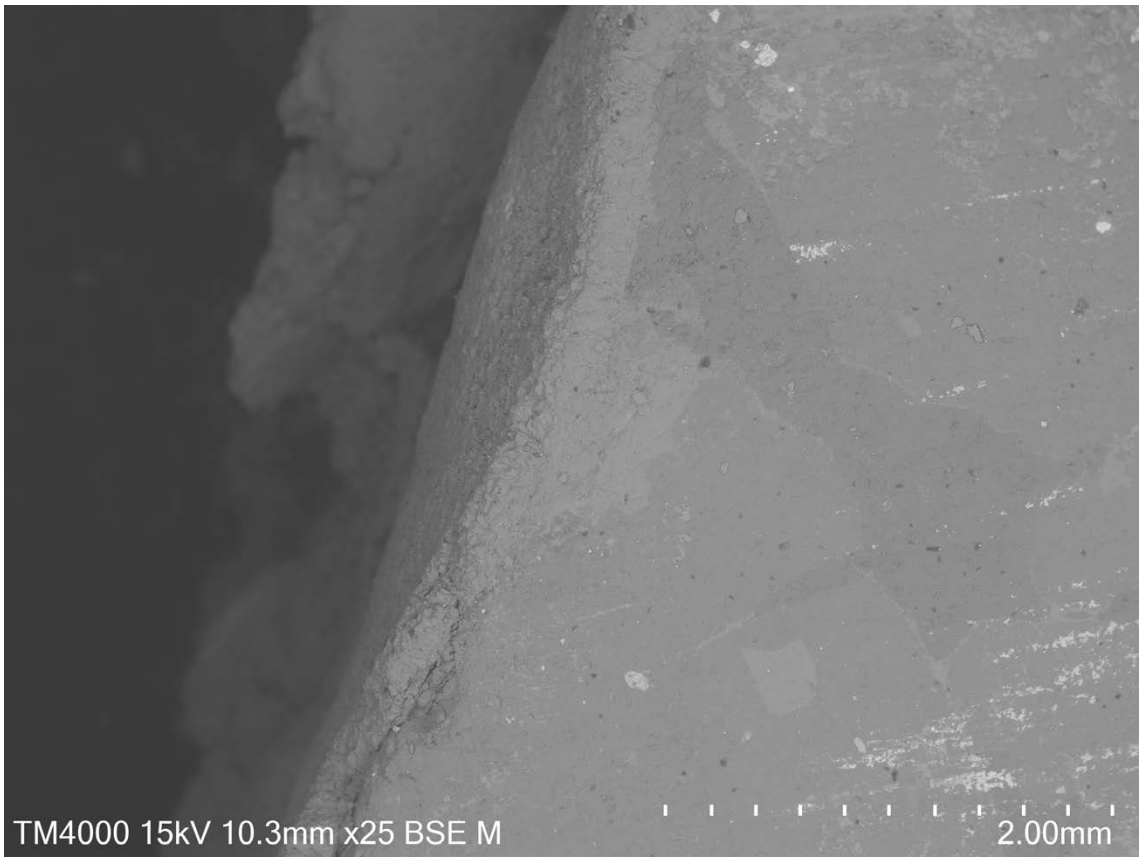

Figure 3-3. *Black surface mineralization from the side (cross-section) in BSE (back scattered electrons) mode. The black surface was located on the left side.*

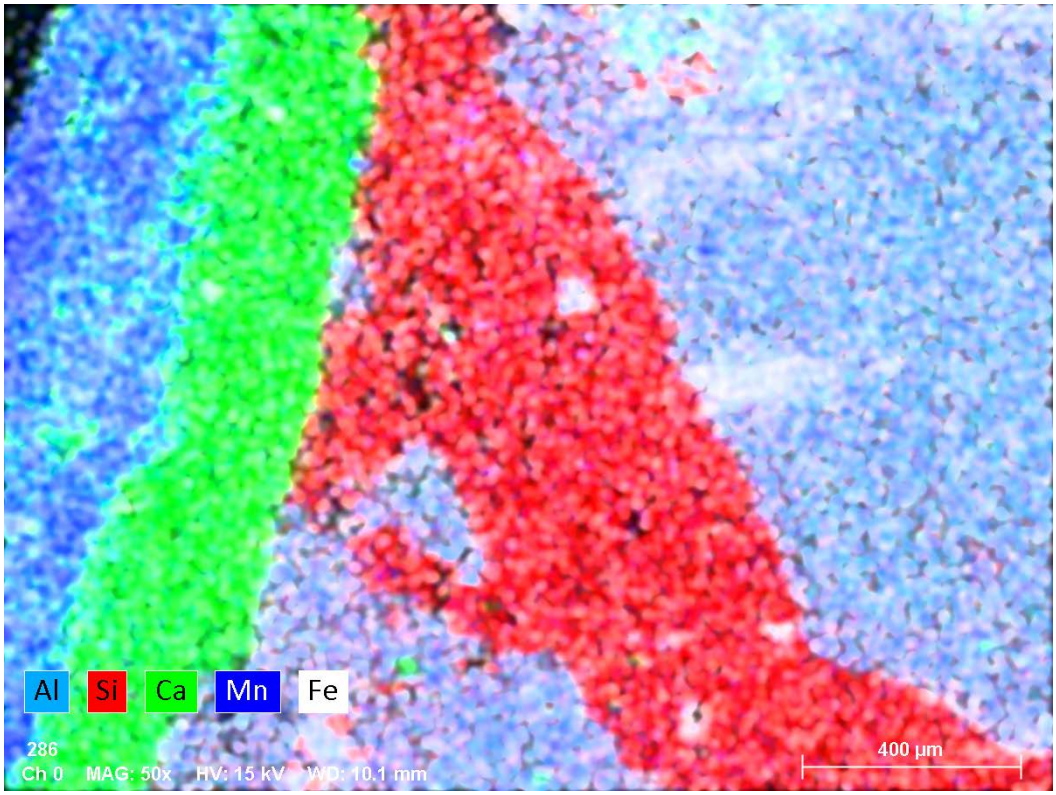

Figure 3-4. *SEM/EDS map of a part of the cross-section shown in Figure 3-3. The black surface was located on the left side and corresponded with the Mn-layer.*

3.2.2 X-ray fluorescence spectroscopy

XRF confirmed that the sample was dominated by Mn and Ca (Table 3-4). Na was not determined with XRF as the elemental content of the sample was determined through a mylar foil.

Table 3-4. XRF data of the sampled black precipitates. All values in wt% (percent by weight).

Sample	MgO	Al_2O_3	SiO_2	P_2O_5	SO_3	Cl
Black precipitates	0.344	0.262	1.193	0.125	0	0.473

	K_2O	CaO	TiO_2	MnO	Fe_2O_3
	0.264	36.143	0.441	57.315	3.44

3.2.3 Powder X-ray diffraction

XRD confirmed that the Ca was associated with calcite and that the Mn-phase in the sample was amorphous or poorly crystalline (Figure. 3-5). Some broad low-angle reflections were seen at 9.8 Å and 7.5 Å that possibly were associated with the Mn-phase (possibly a Mn based layered double hydroxide phase).

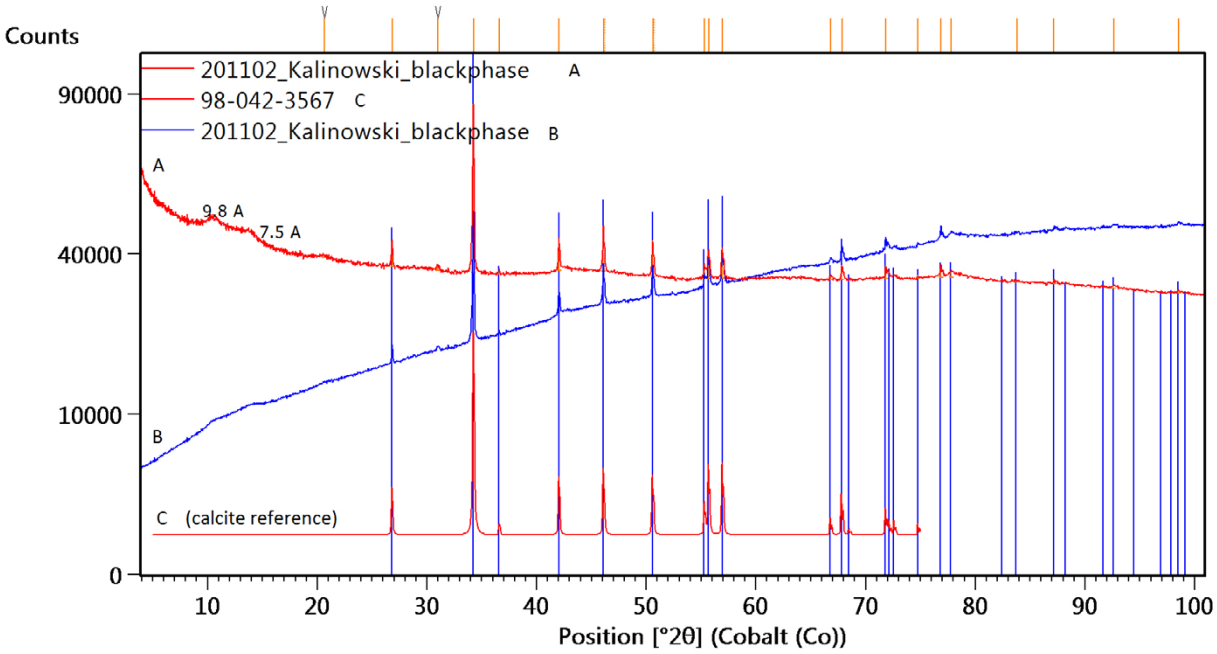

Figure 3-5. *XRD pattern of the sampled black surface. A: Black precipitates (denoted black phase in the figure) with background subtraction. B: Black precipitates with no background subtraction. C: calcite reference data.*

3.3 Microbiology

3.3.1 Microbial cell numbers in TAS04 water samples

Cell numbers in the TAS04 water samples were estimated to be 10^4 to 10^5 cells/mL with a very heterogeneous distribution as most of the cells were attached as cell clusters or biofilms on mineral or precipitates, making it difficult to generate an accurate cell count (Figure 3-6). However, compared to previously analyzed groundwater borehole samples (Lopez-Fernandez et al. 2018b), the cell numbers appear to be slightly increased in this study.

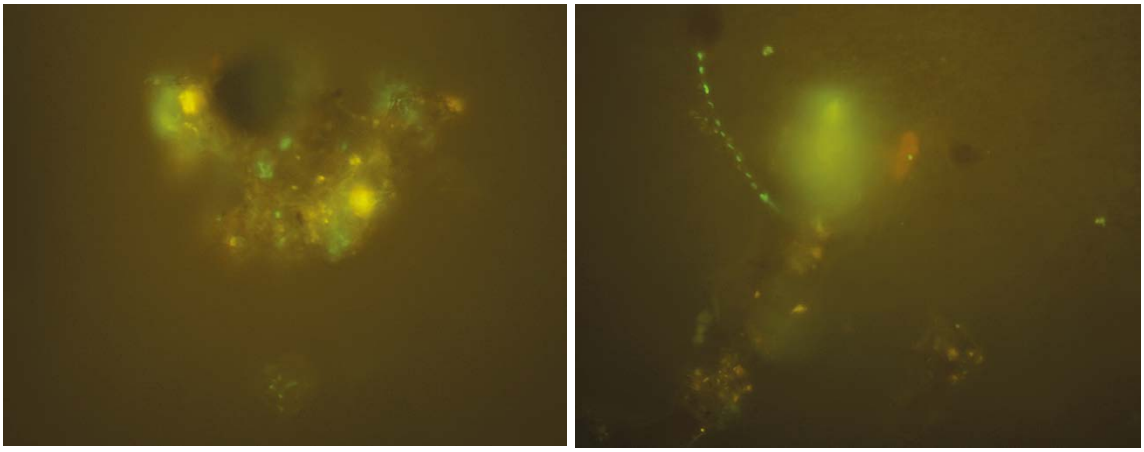

Figure 3-6. *Epifluorescence microscopy images of the 'black water'. Cells are stained green and minerals/ precipitates are the brownish areas. The images have been cropped to show areas of interest.*

3.3.2 16S rRNA gene based microbial community

The rarefaction curves (Figure 3-7) show the number of ASVs against the number of Illumina sequencing reads to estimate if the diversity was covered by the sequencing depth. Most of the samples showed an asymptote converged curve that indicated that the majority of taxa were captured by the sequencing. The number of observed ASVs ranged from 377 to 2 720 (Table 3-5). The estimated richness (Chao1) ranged from 377 to 2 726 while the Shannon diversity index was between 4.95 and 6.38. There was a tendency towards higher richness in the sediment and black precipitates samples compared to the water samples, which could be explained by a higher number of available niches for microorganisms in the solid samples. Overall, the community composition was relatively similar between sites and clusters according to sample type based upon non-metric multidimensional scaling (NMDS) of microbial community composition based on a Bray Curtis dissimilarity (Figure 3-8). A PERMANOVA supported the finding that the community composition was significantly different between sample types ($p = 0.018$). This suggested that the microbial community was selected according to planktonic versus surface bacteria as has been previously reported for Äspö HRL groundwater and biofilm communities (Wu et al. 2017). Comparison of the Shannon indices that ranged from 4.99 in TAS04_RE_S2 to 6.38 in TAS04_RE_S1 (Table 3-5) were in the same range as the Äspö HRL groundwater types (Figure 3-1) that varied from 3.25 in KA2511A to 7.6 in SA1009B (Lopez-Fernandez et al. 2018b).

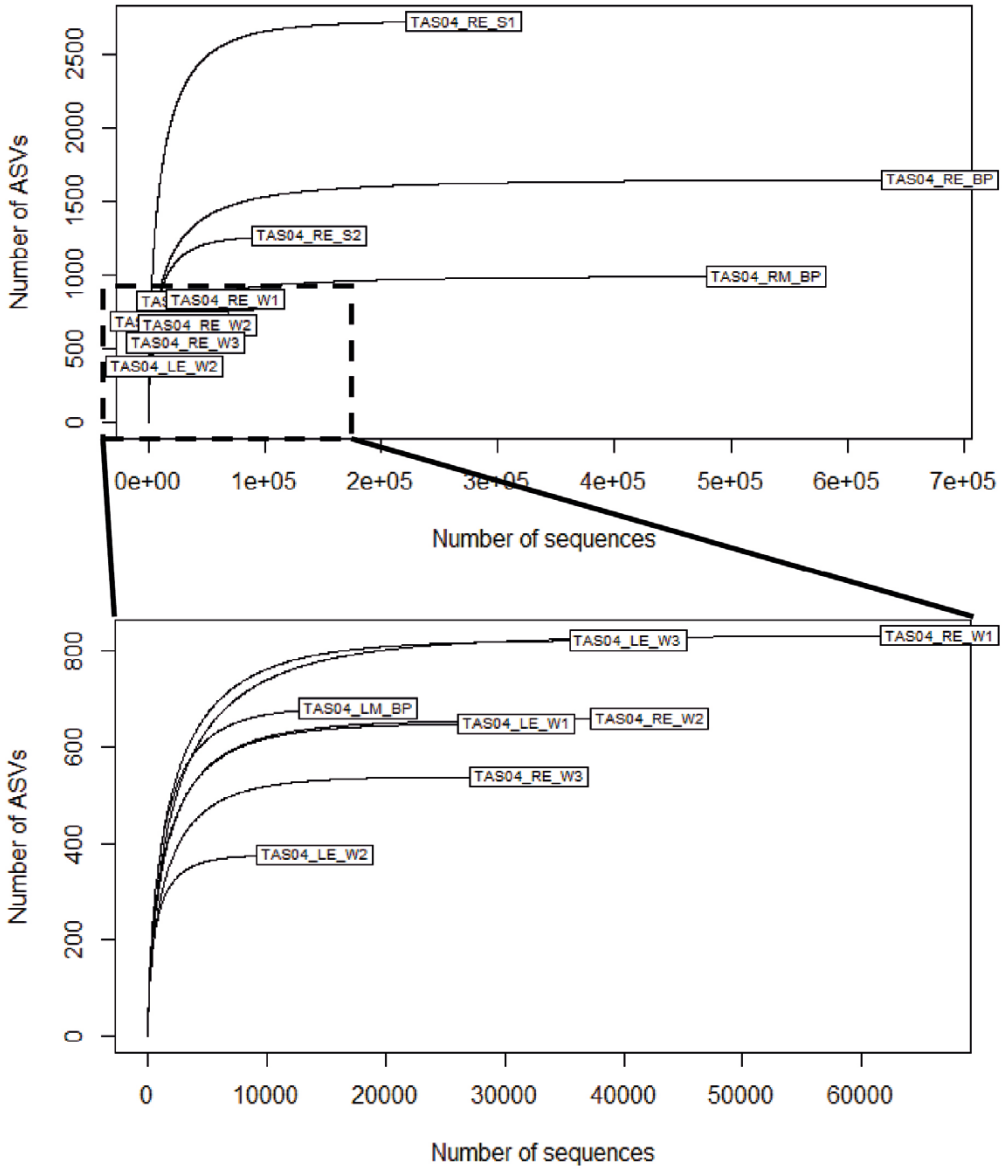

Figure 3-7. *Rarefaction curves showing the sequencing depth for the different TAS04 samples. The upper plot shows all samples, the lower plot shows only the samples with lower number of sequences and ASVs.*

Table 3-5. Alphadiversity: Number of observed ASVs, richness estimator (Chao1), and diversity index (Shannon).

Sample name	No observed ASVs	Chao1	Shannon
TAS04_LE_W1	649	649	5.44
TAS04_LE_W2	377	377	5.18
TAS04_LE_W3	821	824	5.72
TAS04_RE_W1	831	832	5.34
TAS04_RE_W2	659	662	5.30
TAS04_RE_W3	539	539	5.03
TAS04_RE_S1	2720	2726	6.38
TAS04_RE_S2	1263	1268	4.99
TAS04_RE_BP	1643	1644	4.95
TAS04_LM_BP	681	681	5.64
TAS04_RM_BP	987	988	5.41

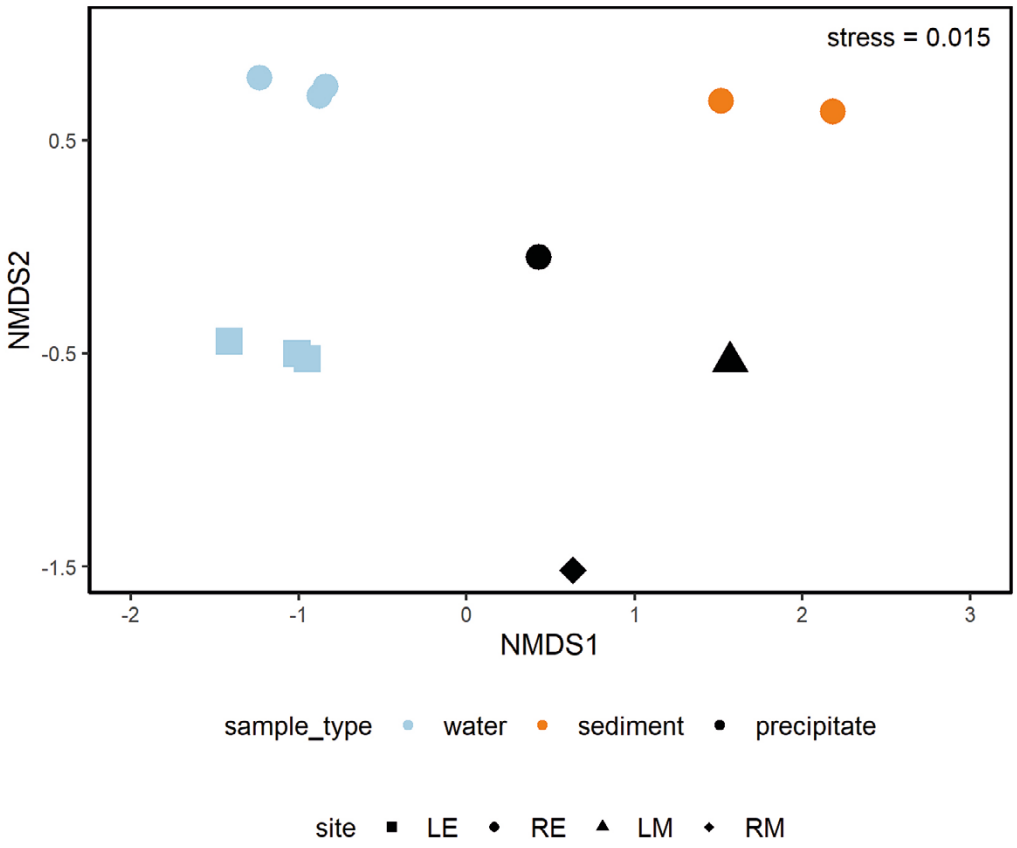

Figure 3-8. *Betadiversity: Non-metric multidimensional scaling (NMDS) of microbial community composition based on a Bray Curtis dissimilarity matrix using relative abundances of the ASVs. Color encodes sample type and shape encodes sampling site.*

The stacked bar graph shows the identified microorganisms in the 'black water' samples on the phylum level (Figure 3-9). In addition, an overview of the abundance of the dominant (i.e. > 1 % of the relative abundance except for at the genus level that is > 0.5 %) populations on family and genus, levels is visualized with balloon plots (Figures 3-10 and 3-11).

The microbial community composition of all sampling sites was dominated by the phylum Proteobacteria (44.6 %; mainly Alpha- and Gammaproteobacteria) along with Planctomycetota (7.3 %), Acidobacteriota (6.3 %), Actinobacteriota (6.1 %), Patescibacteria (5.7 %), and Nitrospirota (3.7 %) (Figure 3-9). The most abundant families were UBA2999, Methyloligellaceae, Hyphomicrobiaceae, and Nitrospiraceae (Figure 3-10).

The data obtained in this study was compared with taxa previously detected in the Ytterby mine, Sweden (Sjöberg 2019) and other studies on known Mn(II)-oxidizers (e.g. Tebo et al. 2005, Cerrato et al. 2010, Piazza et al. 2019)). Overall, the ten most abundant genera were *Methyloligella*, *Gp6-AA40* (Acidobacteriota), *Macondimonas*, *VMFW01* (Patescibacteria), *RKRQ01* (Desulfobacterota_D), *Hyphomicrobium*, *Nitrospira_F*, *Desulfovibrio*, *UBA2100* (Patescibacteria), and *UBA11222* (Alphaproteobacteria) accounting together for a relative abundance of 21.4 % (Figure 3-11). Some of these genera are related to potential Mn(II)-oxidizers. ASVs affiliated to the family Methyloligellaceae, and the genera *Hyphomicrobium* and *Nitrospira* were found to be abundant in the Mn oxides containing black biofilm in Ytterby mine (Sjöberg et al. 2020). Members of the *Hyphomicrobium* genus are well-known Mn(II)-oxidizers (Nealson 2006) and were also identified as potential Mn(II)-oxidizers in enrichments from ferromanganese deposits from a cave (Northup et al. 2003).

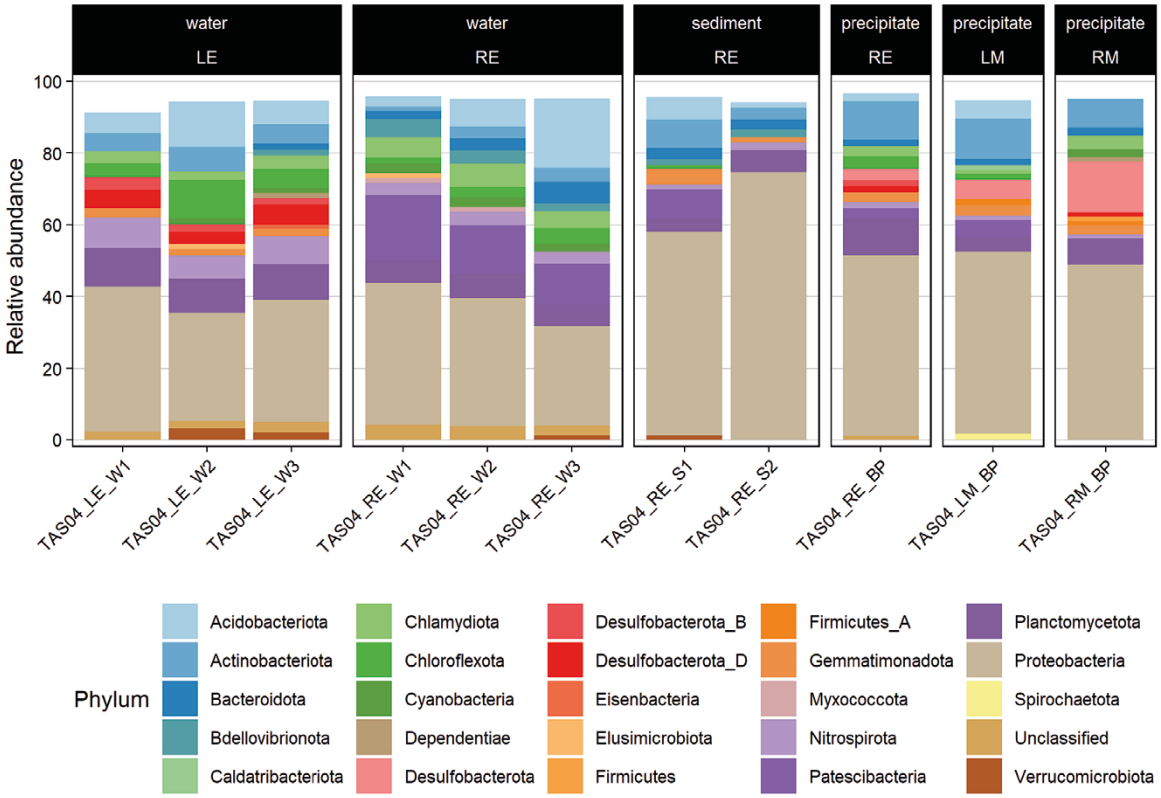

Figure 3-9. *Microbial community composition based on the relative abundances of the phyla with > 1 % abundance in the samples. The remaining proportion to 100 % consists of low-abundant (< 1 %) taxa.*

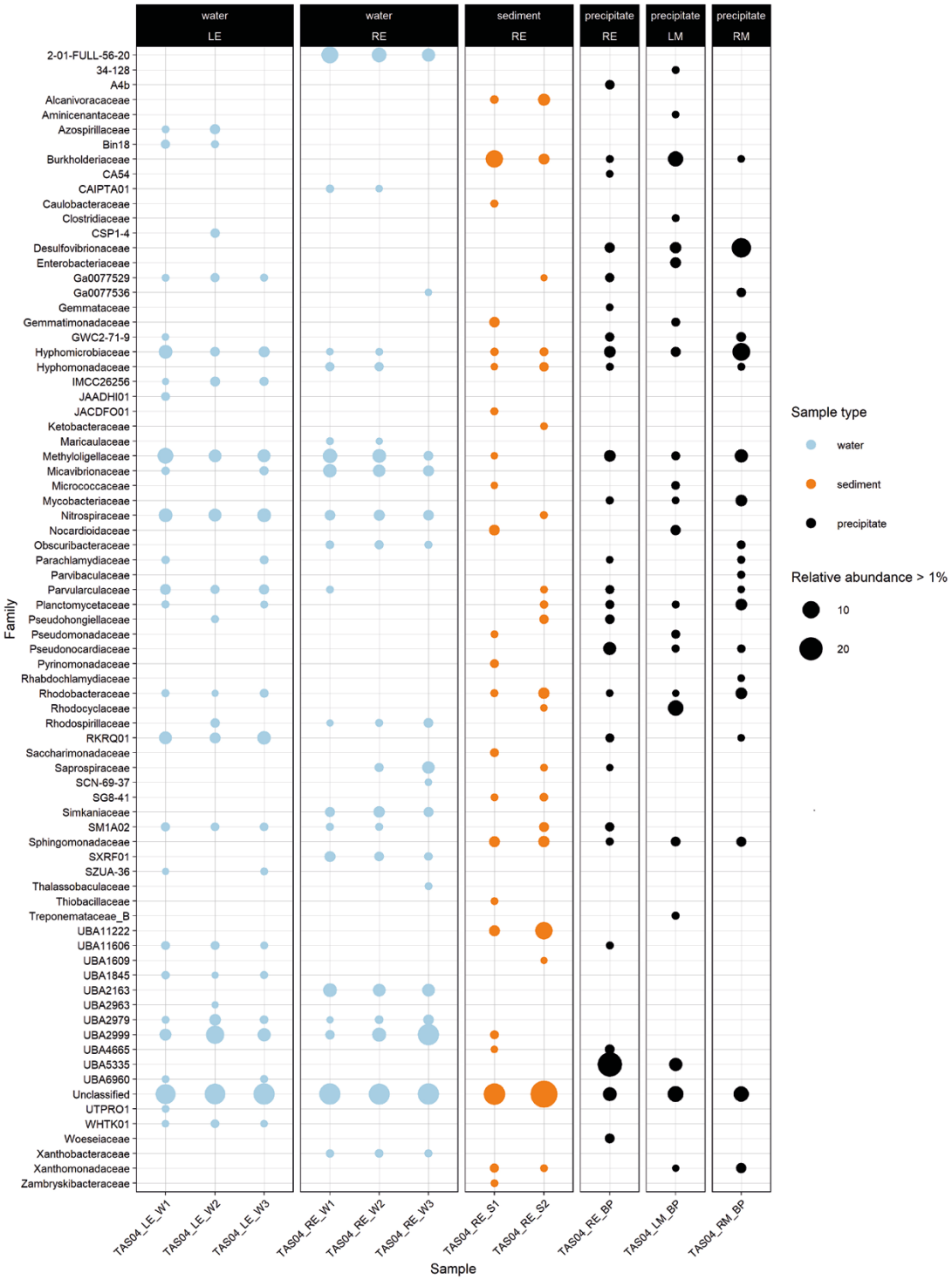

Figure 3-10. *Balloon plot showing the microbial community composition of the water, sediment, and precipitates samples based on the relative abundances of families (> 1 %).*

Further additional genera that have been reported in Mn oxide rich environments or being capable of Mn(II) oxidation in previous studies and that were identified in the present study are listed in Table 3-6 (mean relative abundance > 0.01 %). The genera *Pseudonocardia*, *Hydrogenophaga*, *Mesorhizobium,* and *Reyranella* were present in the Ytterby mine black biofilm (Sjöberg et al. 2020). The Mn(II)-oxidizing bacteria closely related to *Pseudonocardia* sp. and *Mycobacterium* sp. were isolated from Mn nodules of a rice field subsoil (Cahyani et al. 2009). Both genera were found in the TAS04 samples with a higher mean relative abundance in the black precipitates samples compared to their mean relative abundance in all samples. A co-culture of the TAS04 species chemolithoautotrophic *Ramlibacter lithotrophicus* and *Manganitrophus noduliformans* has been shown to use Mn(II) oxidation to fuel growth (Yu and Leadbetter 2020). Bacterial isolates from ferromanganese deposits from a cave and samples from a former uranium mine were thought to be related to Mn(II) oxidation and were affiliated with the genera *Pseudomonas*, *Janthinobacterium*, and *Flavobacterium* (Carmichael et al. 2013, Akob et al. 2014), which were also identified in the TAS04 samples. Two other potential Mn(II)-oxidizers from TAS04 were previously found in freshwater environments – bacteria related to *Brevundimonas* were isolated from biofilms in drinking water systems (Cerrato et al. 2010) and different *Caulobacter* species were isolated from lake water (Gregory and Staley 1982). A bacterial isolate from marine surface sediments closely related to the genus *Erythrobacter*, which is usually characterized as aerobic anoxygenic phototrophs, showed the ability to oxidize Mn(II) (Francis et al. 2001) was detected in TAS04 samples with a very low relative abundance.

Many of the ASVs could not be assigned on genus or species level. Between 12.1–32.9 % of the genera were “unclassified” (Figure 3-10), which reflects the poorly understood deep biosphere communities. Therefore, there might be more novel Mn(II)-oxidizing microorganisms that have not been characterized so far.

The present amplicon sequencing data based on the 16S rRNA gene inform about the microbial community composition and thus, provide limited information with regard to metabolic processes. Therefore, genera and species related to known Mn(II)-oxidizers can be detected, but whether the present strains actually have the potential to oxidize Mn(II) or are active in this environment cannot be inferred from this data.

Table 3-6. Genera found in the TAS04 samples relaled to known Mn(II)-oxidizers or reported in Mn oxide rich environments. Mean relative abundance of potential Mn(II)-oxidizers (> 0.01 %).

Genus	Mean relative abundance – all TAS04 samples (%)	Mean relative abundance – only black precipitates samples (%)
Methyloligella	4.08	3.56
Hyphomicrobium	1.59	3.54
Pseudonocardia	0.88	2.72
Ramlibacter	0.53	0.53
Hydrogenophaga	0.36	0.55
Hyphomicrobium_A	0.34	0.48
Pseudomonas_E	0.32	0.64
Brevundimonas	0.09	0.08
Janthinobacterium	0.08	0.25
Manganitrophus	0.04	0.11
Caulobacter	0.04	0.07
Flavobacterium	0.03	0.09
Mycobacterium	0.03	0.10
Pseudomonas_D	0.03	0.10
Pseudomonas_C	0.03	0.11
Mesorhizobium_E	0.02	0.00
Pseudomonas_A	0.02	0.05
Erythrobacter	0.01	0.03
Erythrobacter_A	0.01	0.01
Reyranella	0.01	0.03

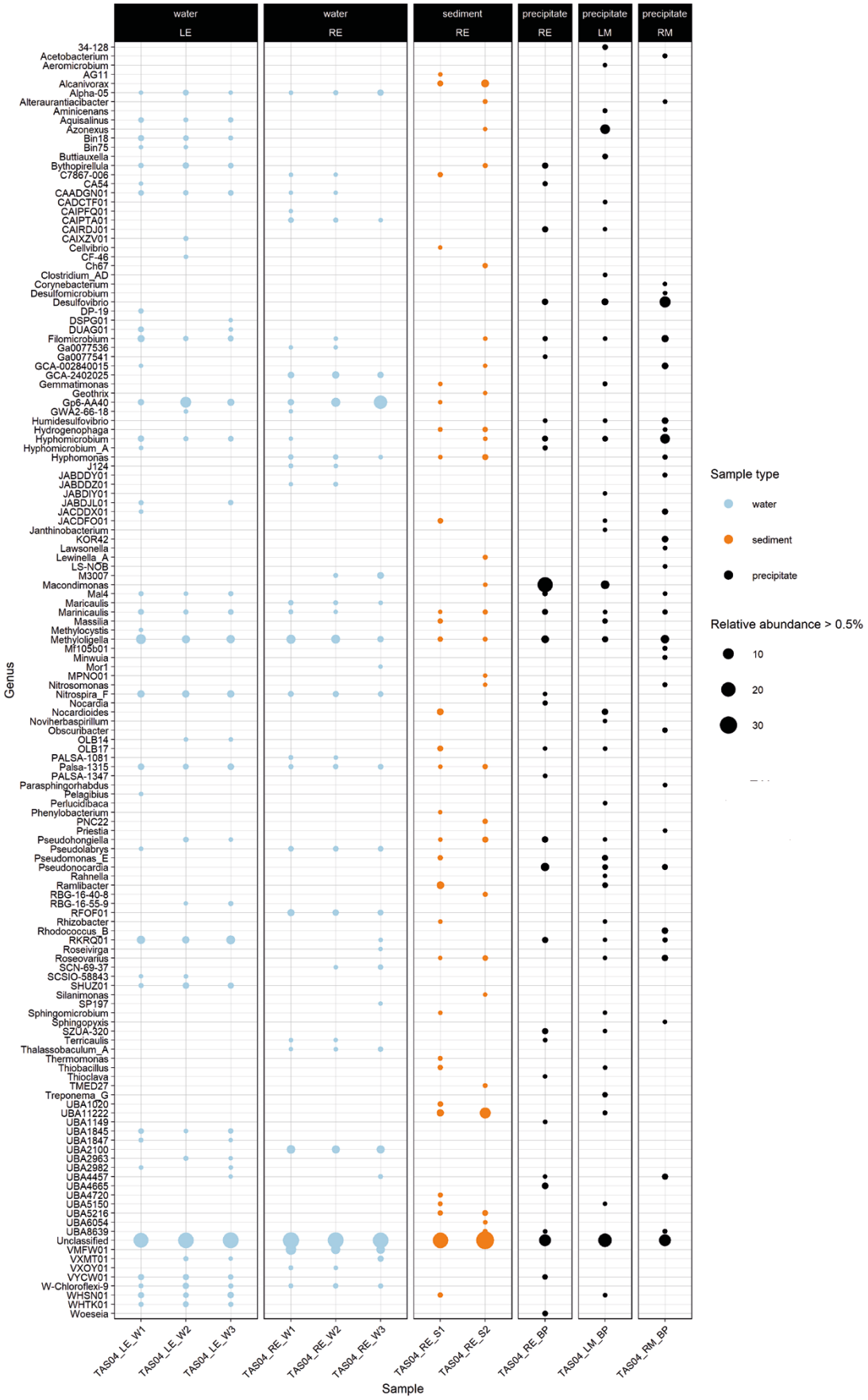

Figure 3-11. *Balloon plot showing the microbial community composition based on the relative abundances of genera (> 0.5 %).*

4 Conclusions

The objectives of this study were to determine the processes causing the black staining of groundwater at several sites in the Äspö tunnel and to characterize the black precipitates causing the staining. It was suggested at an early stage that the black staining of the groundwater could be the result of precipitation of manganese oxide. This assumption was based on previous studies at the Ytterby mine where precipitates of manganese oxides caused black staining of water sipping out from the rock.

Results from the current study indicated that this could also be the case in the Äspö tunnel as the black precipitates on samples taken from TAS04 were confirmed to be enriched in Mn. In addition, the microbiological analysis indicated the presence of Mn(II)-oxidizing bacteria. Further supporting this hypothesis, water from TAS04 was found to have lower Mn levels in comparison to water taken from other boreholes at Äspö, indicating removal of dissolved Mn by precipitation.

References

Akob D M, Bohu T, Beyer A, Schäffner F, Händel M, Johnson C A, Merten D, Büchel G, Totsche K U, Küsel K, 2014. Identification of Mn(II)-oxidizing bacteria from a low-pH contaminated former uranium mine. Applied and Environmental Microbiology 80, 5086–5097.

Cahyani V R, Murase J, Ishibashi E, Asakawa S, Kimura M, 2009. Phylogenetic positions of Mn^{2+}-oxidizing bacteria and fungi isolated from Mn nodules in rice field subsoils. Biology and Fertility of Soils 45, 337–346.

Callahan B J, McMurdie P J, Rosen M J, Han A W, Johnson A J A, Holmes S P, 2016. DADA2: High-resolution sample inference from Illumina amplicon data. Nature Methods 13, 581–583.

Carmichael M J, Carmichael S K, Santelli C M, Strom A, Bräuer S L, 2013. Mn(II)-oxidizing bacteria are abundant and environmentally relevant members of ferromanganese deposits in caves of the upper Tennessee River basin. Geomicrobiology Journal 30, 779–800.

Cerrato J M, Falkinham J O, Dietrich A M, Knocke W R, McKinney C W, Pruden A, 2010. Manganese-oxidizing and – reducing microorganisms isolated from biofilms in chlorinated drinking water systems. Water Research 44, 393–3945.

Francis C A, Co E-M, Tebo B M, 2001. Enzymatic manganese(II) oxidation by a marine α-proteobacterium. Applied and Environmental Microbiology 67, 4024–4029.

Gregory E, Staley J T, 1982. Widespread distribution of ability to oxidize manganese among freshwater bacteria. Applied and Environmental Microbiology 44, 509–511.

Herlemann D P R, Labrenz M, Jürgens K, Bertilsson S, Waniek J J, Andersson A F, 2011. Transitions in bacterial communities along the 2 000 km salinity gradient of the Baltic Sea. The ISME Journal 5, 1571–1579.

Hugerth L W, Wefer H A, Lundin S, Jakobsson H E, Lindberg M, Rodin S, Engstrand L, Andersson A F, 2014. DegePrime, a program for degenerate primer design for broad-taxonomic-range PCR in microbial ecology studies. Applied and Environmental Microbiology 80, 5116–5123.

Lindh M V, Figueroa D, Sjöstedt J, Baltar F, Lundin D, Andersson A, Legrand C, Pinhassi J, 2015. Transplant experiments uncover Baltic Sea basin-specific responses in bacterioplankton community composition and metabolic activities. Frontiers in Microbiology 6. doi:10.3389/fmicb.2015.00223

Lopez-Fernandez M, Broman E, Wu X, Bertilsson S, Dopson M, 2018a. Investigation of viable taxa in the deep terrestrial biosphere suggests high rates of nutrient recycling. FEMS Microbiology Ecology 94. doi:10.1093/femsec/fiy1121

Lopez-Fernandez M, Åström M, Bertilsson S, Dopson M, 2018b. Depth and dissolved organic carbon shape microbial communities in surface influenced but not ancient saline terrestrial aquifers. Frontiers in Microbiology 9. doi:10.3389/fmicb.2018.02880

Mathurin F A, Åström M E, Laaksoharju M, Kalinowski B E, Tullborg E-L, 2012. Effect of tunnel excavation on source and mixing of groundwater in a coastal granitoidic fracture network. Environmental Science & Technology 46, 12779–12786.

Nealson K H, 2006. The manganese-oxidizing bacteria. In Dworkin M, Falkow S, Rosenberg E, Schleifer K-H, Stackebrandt E (eds). The prokaryotes: a handbook on the biology of bacteria. Vol 5: Proteobacteria: alpha and beta subclasses. New York: Springer, 222–231.

Northup D E, Barns S M, Yu L E, Spilde M N, Schelble R T, Dano K E, Crossey L J, Connolly C A, Boston P J, Natvig D O, Dahm C N, 2003. Diverse microbial communities inhabiting ferromanganese deposits in Lechuguilla and Spider Caves. Environmental Microbiology 5, 1071–1086.

Oksanen J, Blanchet F G, Friendly M, Kindt R, P, L, Mcglinn D, Minchin P R, O'Hara R B, Simpson G L, Solymos P, Henry M, Stevens H, Szoecs E, Wagner H, 2020. vegan: Community Ecology Package. R package version 2.5 6.

Parks D H, Chuvochina M, Waite D W, Rinke C, Skarshewski A, Chaumeil P-A, Hugenholtz P, 2018. A standardized bacterial taxonomy based on genome phylogeny substantially revises the tree of life. Nature Biotechnology 36, 996–1004.

Piazza A, Ciancio Casalini L, Pacini V A, Sanguinetti G, Ottado J, Gottig N, 2019. Environmental bacteria involved in manganese(II) oxidation and removal from groundwater. Frontiers in Microbiology 10. doi: 10.3389/fmicb.2019.00119

R Core Team, 2019. R: A language and environment for statistical computing. R Foundation for Statistical Computing, Vienna, Austria. Available at: https://www.r-project.org/ [Accessed version 3.5.3]

Sjöberg S, 2019. Microbially mediated manganese oxides enriched in yttrium and rare earth elements in the Ytterby mine, Sweden. PhD thesis. Stockholm University.

Sjöberg S, Stairs C W, Allard B, Homa F, Martin T, Sjöberg V, Ettema T J G, Dupraz C, 2020. Microbiomes in a manganese oxide producing ecosystem in the Ytterby mine, Sweden: impact on metal mobility. FEMS Microbiology Ecology 96. doi:10.1093/femsec/fiaa1169

Tebo B M, Johnson H A, McCarthy J K, Templeton A S, 2005. Geomicrobiology of manganese(II) oxidation. Trends in Microbiology 13, 421–428.

Wickham H, 2016. ggplot2: elegant graphics for data analysis. 2nd ed. New York: Springer.

Wu X, Pedersen K, Edlund J, Eriksson L, Åström M, Anderson A F, Bertilsson S, Dopson M, 2017. Potential for hydrogen-oxidizing chemolithoautotrophic and diazotrophic populations to initiate biofilm formation in oligotrophic, deep terrestrial subsurface waters. Microbiome 5. doi:10.1186/s40168-40017-40253-y

Yu H, Leadbetter J R, 2020. Bacterial chemolithoautotrophy via manganese oxidation. Nature 583, 453–458.

Arkitektkopia AB, Bromma, 2022

SKB is responsible for managing spent nuclear fuel and radioactive waste produced by the Swedish nuclear power plants such that man and the environment are protected in the near and distant future.

skb.se